Steel and Composite Structures, *Vol. 19, No. 5 (2015) 1095-1113*
DOI: http://dx.doi.org/10.12989/scs.2015.19.5.1095

Mechanical behavior of the composite curved laminates in practical applications

Lonquan Liu [*1], Junqi Zhang [1], Hai Wang [1] and Zhongwei Guan [2]

[1] *School of Aeronautics and Astronautics, Shanghai Jiao Tong University, Shanghai, P.R. China*
[2] *School of Engineering, University of Liverpool, Brownlow Street, Liverpool L69 3GQ, UK*

(*Received January 05, 2014, Revised May 10, 2014, Accepted April 18, 2015*)

Abstract. In order to determine the mechanical behavior of the curved laminates in practical applications, three right-angled composite brackets with different lay-ups were investigated both experimentally and numerically. In the experimental, quasi-static tests on both unidirectional and multidirectional curved composite brackets were conducted to study the progressive failure and failure modes of the curved laminates. In the numerical modeling, three-dimensional finite element analysis was used to simulate the mechanical behavior of the laminates. Here, a strength-based failure criterion, namely the Ye criterion, was used to predict the delamination failure in the composite curved laminates. The mechanical responses of the laminate subjected to off-axis tensile loading were analyzed, which include the progressive failure, the failure locations, the load-displacement relationships, the load-strain relationships, and the stress distribution around the curved region of the angled bracket. Subsequently, the effects of stacking sequence and thickness on the load carrying capacity and the stiffness of the laminates were discussed in detail. Through the experimental observation and analysis, it was found that the failure mode of all the specimens is delamination, which is initiated abruptly and develops unstably on the symmetric plane, close to the inner surface, and about 29° along the circumferential direction. It was also found that the stacking sequence and the thickness have significant influences on both the load carrying capacity and the stiffness of the laminates. However, the thickness effect is less than that on the curved aluminum plate.

Keywords: curved laminate; mechanical behavior; finite element; stacking sequence; delamination

1. Introduction

Composite materials are increasingly replacing metallic alloys in aircraft due to their contribution to weight savings and improved durability. Without exception, the shear ties, which are usually used to transfer the aerodynamic loads from the skin panes into the ribs and spars of the aircraft wing, are also made of composite materials through some of the current aircraft designs.

However, process induced residual stresses, deformations, and thickness variations around the curved region are important concerns in terms of the mechanical performance of L-shaped composite structures, since these defects can lead to a reduction of the strength and fatigue life,

*Corresponding author, Ph.D., E-mail: liulongquan76@sjtu.edu.cn

http://www.techno-press.org/?journal=scs&subpage=8 ISSN: 1229-9367 (Print), 1598-6233 (Online)

and can initiate cracks in the matrix. Many scholars have focused on optimizing the manufacturing process to eliminate or decrease the induced defects of the curved laminates (Miao *et al*. 2013, Sorrentino and Bellini 2013, Sun *et al*. 2013, Shimizu and Abe 2013). However, even the curved laminates are built perfectly without any defect, they are still weak in practical applications due to the prime failure mode of delamination. This is because on the one hand the laminates have comparatively low through-the-thickness (TTT) strength, on the other hand, there are high interlaminar stresses arisen from the material discontinuities, geometric discontinuities and eccentricities in the loading path. A better understanding of the stress distribution around the curved region and how the different parameters influence the load carrying capacity of the curved laminates is important and necessary to help optimize the design.

Extensive work was undertaken to study the mechanical behavior of curved laminates by using analytical approaches. For example, a closed form solution for the elasticity of curved laminate under pure end moment and force was provided by Lekhnitskii (1987). Lin and Hsieh (2007, 2011) also developed closed form solutions for the curved laminates and presented the mathematical expressions for the curved laminate with different curvatures under axial, shearing, radial and tangential loads. The analytical results are comparable with the numerical simulations. Lin (2010) proposed an analytical method for obtaining the finite deformation of two-dimensional thin curved laminated beam, through which the solutions agree with the numerical results by using ANSYS software. However, the closed form method is only suitable to obtain the mechanical responses of the curved laminates under ideal working states, which is incapable of solving the failure mechanisms and dealing with the nonlinear characteristics of the curved laminates. As the results, it is difficult to consider the influence the stacking sequence, the defects, the nonlinear deformations and the connections with other composites.

Since the failure mode of the curved laminate is mainly interlaminar delamination, many scholars have developed test methods to measure the interlaminar mechanical properties of the composite materials (Wisnow *et al*. 1996, Wan *et al*. 2013, Cui *et al*. 1996). For example, Wan *et al*. (2013) conducted tensile tests on the L-shaped laminates to evaluate the strength and fracture behavior of the curved section of the CF/PP. By referring to ASTM D6415 test standard (2007), Cui *et al*. (1996) proposed a method to measure the interlaminar tensile strength of curved beam specimens using four-point bending. However, these test configurations did not match with the practical loading conditions exactly and these studies only focused on the basic performance of the curved laminates with the actual load bearing conditions ignored.

In fact, the failure of curved laminates is mainly dependent on the stress state around the curved region. Therefore, to obtain the stress distributions in curved laminates is essential to predict their its strength. For example, Joh (1990) measured the strain distributions of the curved laminate using the Moire interferometry whole-field optical method. However, the curved brackets normally are very thin and the measuring area is very narrow, which restricts the application of the optical method in measuring the real stress distribution in the curved region along the thickness direction. Moreover, the test method is expensive and time consuming.

Chang and Springer (1986) undertook a numerical study on the failure load of a L-shaped beam triggered by delamination. Wimmer *et al*. (2009) investigated both the initiation and propagation phases of delamination using the implicit solver of the Abaqus software. Roos (2008) proposed a mechanical model to calculate the interlaminar normal stress in thick-walled singly and doubly curved laminates. The analytical model provided accurate results in consideration of the significant simplifications. Moreover, the finite element (FE) simulations were used to predict the maximum delamination load which was validated by delamination strength tests. Nguyen (2010) developed

3-D finite element models of the curved laminated beams using PATRAN/NASTRAN. He studied the variation of both tangential and radial stresses with respect to the changing in curvature, stacking sequence and fiber orientation in a curved laminated beam subjected to a bending moment.

From the above review, it can be seen that both the analytical method and the test method have their own shortcomings. Comparatively, the finite element modeling, once it is validated against the related experimental results, can not only obtain the stress and strain status inside the composite material, but also to save the research cost and time, which make it as an indispensable tool for the structural design. This paper presents a study on the mechanical behavior of the curved laminates under shear loading by using the FE modeling validated with test results. Here, both the unidirectional and multidirectional composite curved laminates are investigated. The output covers load-displacement curves, failure initiation, failure mode, stress distribution and the effects of stacking sequence and thickness of the laminates.

2. Experimental studies

2.1 Specimens description

A typical usage of the curved composite shear tie is shown in Fig. 1, in which the shear tie is used to connect the rib and the skin pane together. Here, the four sets of fasteners are used to connect the shear tie with the stiffened skin panel and the rib together. Shear ties have a complex curved shape and specific load carrying requirements. Under service loads, the final failure mode

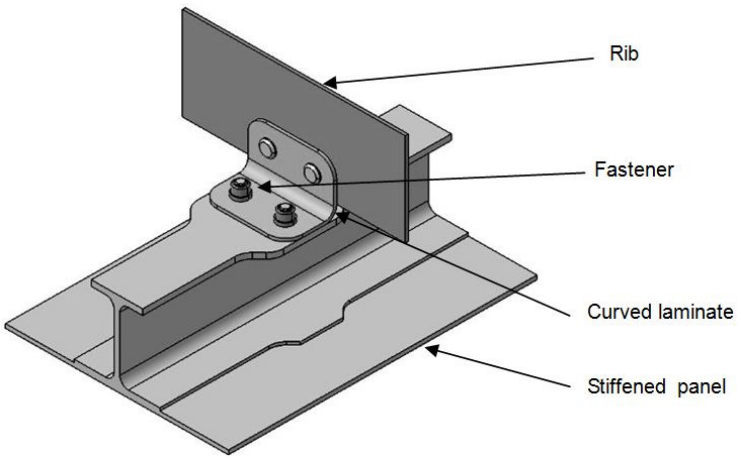

Fig. 1 Joints structure of frame and skin

Table 1 Specimen configurations

Specimen No.	Stacking sequence	Thickness (mm)
Specimen-1	$[0]_{14}$	2.632
Specimen-2	$[+/-45]_7$	2.632
Specimen-3	$[+/-45,0_2,90, 0_2,-/+45, +/-45, 90, 0,-45]$	2.632

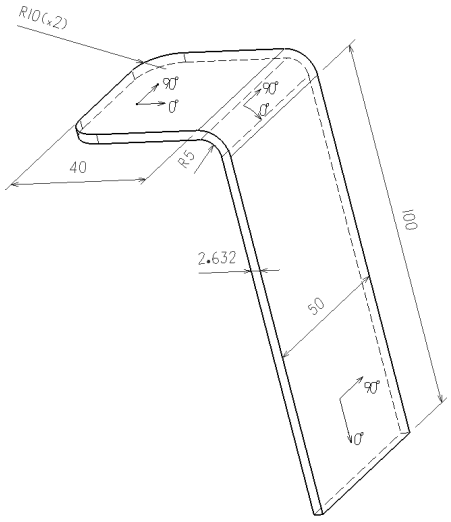

Fig. 2 Geometry and dimensions of the specimen (all dimensions in mm)

of the curved laminated composite shear ties is usually found to be delamination.

To investigate the mechanical behavior of the composite shear ties under service, three different curved laminates were tested in this research. All the curved laminates are made of Cytec carbon fiber epoxy unidirectional lamina, whose nominal cured ply thicknesses is 0.188 mm, and the configurations of specimens are shown in Table 1.

All the geometry and dimensions of the three different batches of specimens are the same, which are shown in Fig. 2. All the three different specimens have 5 mm inner radius, 40 mm long arm, 150 mm long leg, and 50 mm width. The tolerances of locations and dimensions in Fig. 2 conform to the general tolerance requirements for composite products HB 7741-2004.

The mechanical properties of the unidirectional lamina are shown in Table 2. Here, the "1", "2" and "3" directions are the longitudinal, transverse and thickness directions of the unidirectional tape lamina. Those three directions of the unidirectional tape lamina with 0 degree are coincident with the 0°, 90°, and thickness directions of the coordinate system shown in Fig. 2, respectively.

In Table 2, E_{ij} (i, j = 1,2) are the elastic modulus of the unidirectional tape lamina in longitude and transverse directions. G_{ij} (i, j = 1,2,3) are the shear modulus, υ_{ij} (i, j = 1,2,3) are the Poisson's ratios, and S_{ij} (i, j = 1,2,3) are the material strengths. The superscript T and C denote tension and compression, respectively. Since the properties of the composite through its thickness are very difficult to obtain, it is customarily assumed that the matrix properties are applied in the thickness direction (Mukundan 2003). Therefore, it can be said that $E_{22} = E_{33}$, $G_{12} = G_{13}$, $v_{21} = v_{31}$, $S_{22} = S_{33}$ and $S_{12} = S_{13}$ are applied to the unidirectional lamina.

Table 2 Mechanical properties of the unidirectional tape lamina

Elastic property	E_{11} (GPa)	E_{22} (GPa)	G_{12} (GPa)	G_{23} (GPa)	v_{12}	v_{23}
Value	175	8.03	4370	2875	0.32	0.4
Strength property	S_{11}^T (MPa)	S_{11}^C (MPa)	S_{22}^T (MPa)	S_{22}^C (MPa)	S_{12} (MPa)	S_{23} (MPa)
Value	2786	1602	62.4	212.8	111.9	36.5

2.2 Test setup

Three batches of specimens (six in each batch) described in Table 1 were quasi-statically tested by using a MTS electron-hydraulic servo-controlled material testing machine, as shown in Fig. 3. Fig. 3(a) illustrates the specimen attaching to the material testing machine, whilst Fig. 3(b) shows the specimen modification to connect to the testing machine, and Fig. 3(c) shows the strain gauges used to align the specimens. The end of the curved laminate leg is clamped by the stationary head of the testing machine, and the grip length is 20 mm. To connect the curved laminate together with the movable head of the testing machine, two holes with 6 mm diameter are drilled on the arm of the specimen. The arm of curved laminate is connected with the "rigid" *jig* through two sets of M5 fasteners, and the *jig* is clamped together with the movable head of the testing machine. The quasi-static tensile tests were performed in displacement control mode at a constant speed of 1 mm/min. The tests were terminated when the stiffness was lost. The circumstance temperature was maintained to be within 23 ± 5 degree Celsius, and the relative humidity was within 55 ± 5% during test. The edge surfaces of the specimens were painted with brittle white or red paint to aid in detecting matrix cracks or delaminations. The four strain gauges shown in Fig. 3(c) were used to measure the strain values and to adjust the alignment of the specimens.

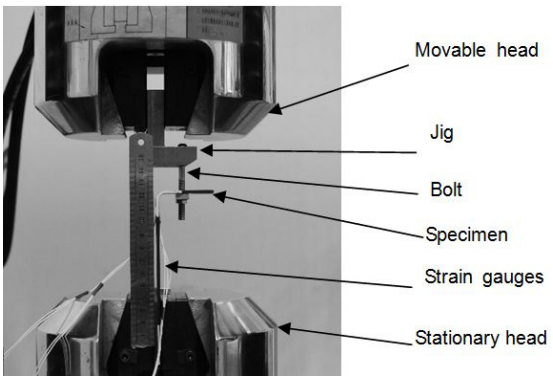

(a) Specimen installation

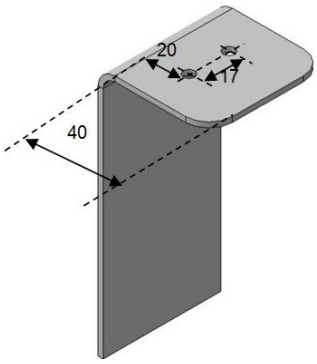

(b) Connection holes on specimens

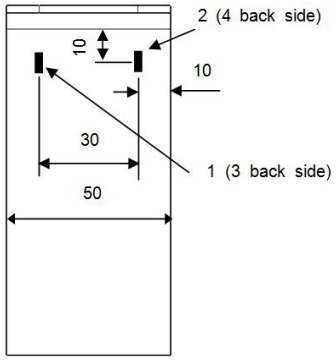

(c) Location of stain gauges

Fig. 3 Test setup (all dimensions in mm)

(a) Specimen-1 (b) Specimen-2 (c) Specimen-3

Fig. 4 Failure modes of the specimens

2.3 Test phenomena

There was no audible sound before failure, however there was a loud noise emitted when the specimens fail. Delamination is typically accompanied by a sharp decrease in force and a lost in stiffness. The failure modes of the three kinds of specimens are shown in Fig. 4. The failure mode of all the specimens is delamination in the curved region, which is extended to all over the 90° curved angle instantaneously after the delamination is initiated.

There is mainly one delamination located close to the inner radius of the specimen-1 and specimen-2. However, there are two delaminations in the curved region of the specimen-3, which almost separate the curved laminate into three parts in the thickness direction, with the outer delamination open wider than the inner one.

3. Numerical studies

3.1 Three-dimensional model

3.1.1 Meshes

To simulate the structural behavior of the curved laminates, a three-dimensional (3D) finite element is developed using commercial finite element code Abaqus/standard (Hibbitt *et al*. 2011), which is shown in Fig. 5. Due to the symmetric features of the structure, ply sequence, and boundary conditions with respect to XY plane shown in Fig. 5, only half of the joint is modeled. Therefore, the curved laminate modeled as 25 mm wide. The leg of the curved laminate modeled as 80 mm long since 20 mm of the 100 mm long leg are clamped by the stationary head of the testing machine. Since the stiffness of the jig is much higher than that of the specimen, the *jig* is treated as rigid body with a reference point.

In Abaqus software, the hexahedral elements use either “full” or “reduced” integration to allow complete generality in material behavior. For full integration the number of integration points is sufficient to integrate the virtual work expression exactly, at least for linear material behavior. Most fully integrated solid elements are unsuitable for the analysis of (approximately) incompressible material behavior as the material behavior forces the material to deform (approximately) without volume changes. Comparing with the full integration, the advantage of the reduced integration elements is that the strains and stresses are calculated at the locations that

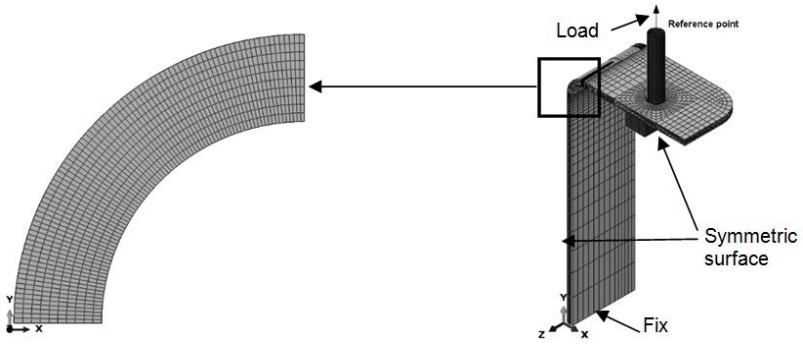

(a) Detail view (b) FE model

Fig. 5 Finite element model of Fabric-1 subjected to tensile load

provide optimal accuracy, the so-called Barlow points. A second advantage is that the reduced umber of integration points decreases CPU time and storage requirements. However, the isadvantage of the reduced integration elements is that the reduced integration procedure can admit deformation modes that cause no straining at the integration points. These zero-energy modes make the element rank-deficient and cause a phenomenon called "hourglassing," where the zero energy mode starts propagating through the mesh, leading to inaccurate solutions (Mukundan 2003). To prevent these excessive deformations, an additional artificial stiffness is added to the element. In this so-called hourglass control procedure, a small artificial stiffness is associated with the zero-energy deformation modes. Therefore, the enhanced hourglass control and reduced integration linear eight-node brick elements, C3D8R, are used to model each ply of the laminate and the fasteners to avoid shear locking problem, to simulate the bending deformation introduced by the secondary bending effect more accurately, and to decrease the computing time. The curved laminate was modeled using 31290 elements and 36060 nodes, and the fastener using 10808 elements and 12605 nodes.

The modeling method of one element per ply thickness of the curved laminate provides a reasonable approximation of the through-thickness stresses. The modeling method of one element per one degree sweeping around the curved region provides accurate stress predictions along the circumstantial direction in the curved region, that is to say that there are totally 90 elements distributed along the circumstantial direction and 14 elements along the width direction around the curved region. The mesh density and aspect ratio in the contact area between the fastener and curved laminate are to affect the convergence of the simulation results and therefore, the meshes in these areas are more refined than those in other areas. Thirty-two elements are equally distributed on the periphery of the fastener hole along circumferential direction, which is similar to the mesh convergence results from Rosales-Iriarte *et al*. (2012) and Padhi *et al*. (2002).

3.1.2 Boundary constraints

The nodes at the end of the leg of the specimen are held fixed in all three translational directions (U_x, U_y and U_z). The symmetry surface of the specimen is constrained in translational direction U_z. The top surface of the fastener is declared as a rigid body and has pin relationship with a reference node. Thus, the motion of the top surface is governed by the motion of the reference node, which is held fixed in two translational directions (U_x and U_z) and three rotational

directions (R_x, R_y and R_z), while a pull load is applied along U_y direction.

3.1.3 Contact definition

The contact relationships in the joints are defined between the fastener and the curved laminate. Because the nut and fastener shank are engaged together, they are modelled as one part to decrease the contact surfaces and shorten the CPU time. Finite sliding formulation is used to model the contact relationship between the fastener and the curved laminate. The frictional coefficient between titanium materials is set to be 0.4 and that between the titanium material and composite material is set to be 0.1 according to the results of Herrington and Sabbaghian (1991).

3.1.4 Material properties and failure criteria

The primary failure modes of the unidirectional tape lamina include fiber tensile/compression failure, matrix tensile/compression failure and delamination. Generally, progressive failure analysis consists of two major steps (Ng *et al*. 2001). The first step is to choose appropriate failure criteria to justify which kind of failure mode occurs prior to others. Since the only failure mode of the specimens is delamination between the layers of the curved laminates, the three-dimensional Ye (1988) delamination criterion is applied in the finite element model to predict the failure of the specimens, which is illustrated as in Eqs. (1) and (2).

$$\left(\frac{\sigma_{33}}{S_{33}^T}\right)^2+\left(\frac{\sigma_{13}}{S_{13}^T}\right)^2+\left(\frac{\sigma_{23}}{S_{23}^T}\right)^2 \geq 1, \sigma_{33} \geq 0 \tag{1}$$

$$\left(\frac{\sigma_{13}}{S_{13}^C}\right)^2+\left(\frac{\sigma_{23}}{S_{23}^C}\right)^2 \geq 1, \sigma_{33} \leq 0 \tag{2}$$

where σ_{ij} (i, j = 1,2,3) are the stress components of the unidirectional tape lamina in the longitudinal and transverse directions.

Delamination occurs between different element layers when the average stress of the elements surrounding the specified integration point satisfy the Ye criterion.

3.2 Results analysis

3.2.1 Load-displacement curves

The load-displacement curves of the typical test results and simulation results are shown in Fig. 6. Figs. 6(a)-(c) illustrate the load-displacement curves of the specimen-1, specimen-2, and specimen-3 described in Table 1, respectively. From the Fig. 6, it can be seen that the simulation results agree with the test results quite well with regard to the stiffness and strength of the curved laminate. The load carrying capacities obtained from the test results are lower than those obtained from the simulation results, and this is partly due to the simulation did not consider the manufacturing inconsistency and quality of the curved laminates. From Fig. 6, it can also be seen that the testing loads of the specimens drop abruptly without any warning signs and the stiffness keeps increasing before it decreases to zero suddenly, which means the curved laminate fails suddenly in the loading process.

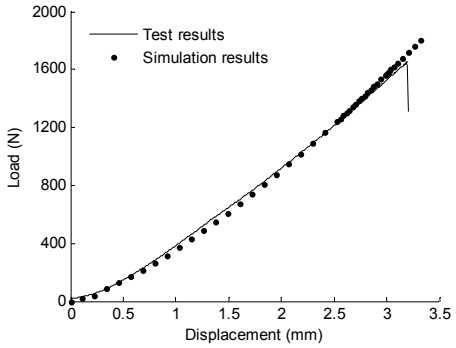

(a) Specimen-1

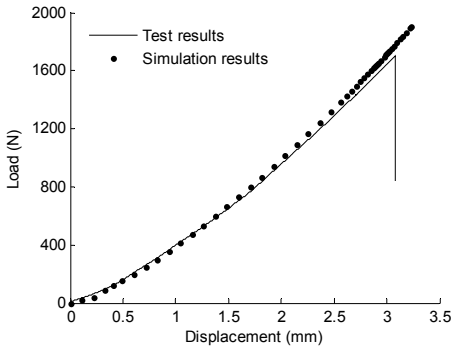

(b) Specimen-2

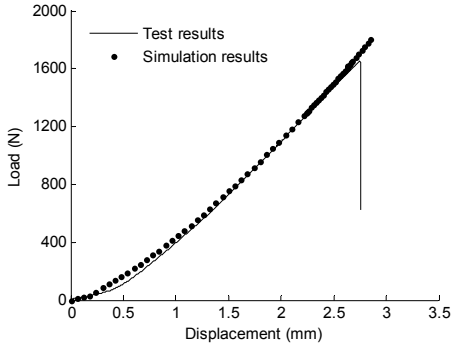

(c) Specimen-3

Fig. 6 Comparison of load-displacement curves between test and simulation results

3.2.2 Load-strain curves

Fig. 7 illustrates the load-strain relationships of the three curved laminates in the loading rocess. Figs. 7(a)-(c) illustrate the load-strain curves of the specimen-1, specimen-1, and specimen-3, respectively. The legends “strain1-test” and “strain3-test” represent the measured strains at point 1 and point 3, shown in Fig. 3; the legends “strain1-FE” and “strain3-test” represent the simulated strains of point 1 and point 3, respectively. From the Fig. 7, it can be seen that the simulation results match with the test results generally.

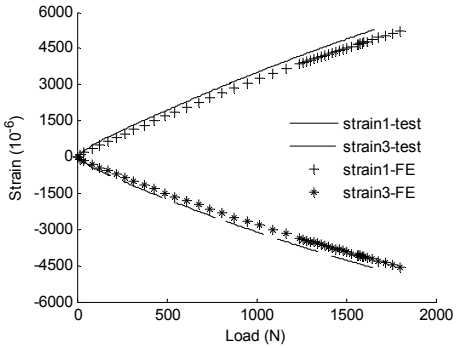

(a) Specimen-1

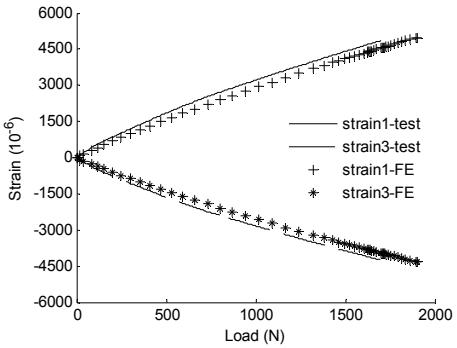

(b) Specimen-2

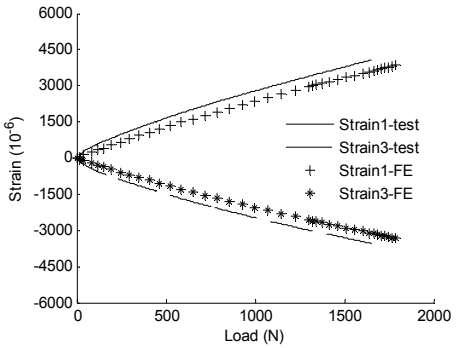

(c) Specimen-3

Fig. 7 Comparison of load-strain curves between test and simulation results

3.2.3 Stress distributions

To study the stress distributions of the curved laminate, a cylindrical coordinate system was created, as shown in Fig. 8. r_i is the inner radius and r_o is the outer radius of the curved laminate, t is the thickness of the laminate. The "R", "φ" and "Z" directions of the cylindrical coordinate system shown in Fig. 8 are identical with the "3", "1" and "2" directions of the lamina with 0^o ply angle. Each point in the curved region can be defined by r and θ in the cylindrical coordinate system. According to Eqs. (1)-(2), the delamination is dependent on the stress components of σ_{33},

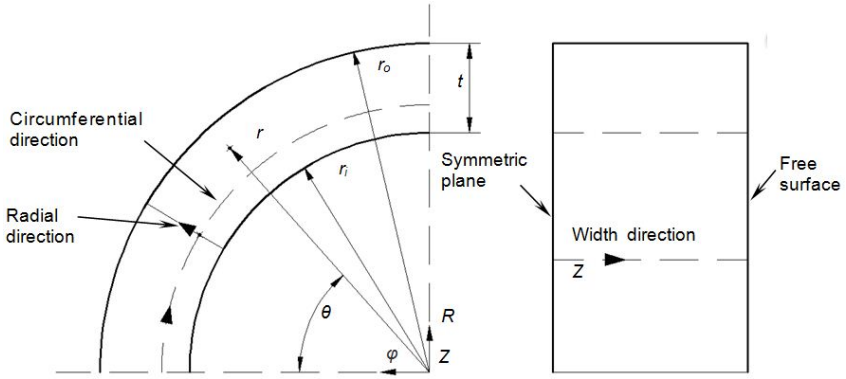

Fig. 8 Notation of the location in the curved region

σ_{13}, and σ_{23}. Thus, these three stress components of the elements along three paths are used to illustrate the stress distributions around the curved region. The three paths are in the width, thickness and circumferential directions, respectively (Fig. 8). The intersection point of the three paths is at the location of the element that will fail first in the loading process according to the Eqs. (1) and (2). As for the specimen-1, the failure initiates at the location of r = 6.13 mm, θ = 29° and Z = 0 mm. As for the specimen-2 and Specimen-3, the failure both initiates at the location of r = 5.94 mm, θ = 28° and Z = 0 mm.

1) The stress distributions along the width direction

The distributions of three stress components, σ_{33}, σ_{13}, and σ_{23}, of the three curved laminates with different stacking sequences along the width direction (the Z direction shown in Fig. 8, which is from the symmetric plane to the free surface) are shown in Fig. 9. Here, the width ratio is defined by the ratio between the distances of the relevant element to the symmetric plane and half of the width of the curved laminate, 25 mm.

Figs. 9(a)-(c) show the stress distributions of the specimen-1, specimen-2 and specimen-3, respectively. From the Fig. 9, it can be seen that the σ_{33} of all three specimens are higher than the σ_{13}, and σ_{23}. Here, the onset of the delamination is mainly dominated by mode I crack. The σ_{13} of all three specimens are very low, about 5 MPa. The σ_{23} of the specimen-1 and specimen-3 are even lower than the σ_{13}. However, the σ_{23} of the specimen-2 is quite high, with the maximum value of about 30 MPa, which means the mode II crack introduced by the σ_{23} plays some effect on the delamination of the curved laminate with $[+/45]_7$ lay-up.

The σ_{33} of all three specimens decreases with the increase of the width ratio and the σ_{23} of specimen-2 decreases with the increase of such the ratio. This means that the onset of the delamination should be on the middle plane (the symmetric plane shown in Fig. 5(c)) of the curved laminate but not on the free surface.

The stress around the curved region of the right-angled laminate is thought to be identical according to the closed form solution proposed by Lekhnistskii (1987) and the 2D and 3D FEM proposed by Wan *et al*. (2013). Therefore, their methods are not suitable to accurately predict the stress state inside the curved laminates in practical applications.

2) The stress distributions along the radial direction

Fig. 10 shows the distributions of the stress components, σ_{33}, σ_{13}, and σ_{23}, on the symmetric

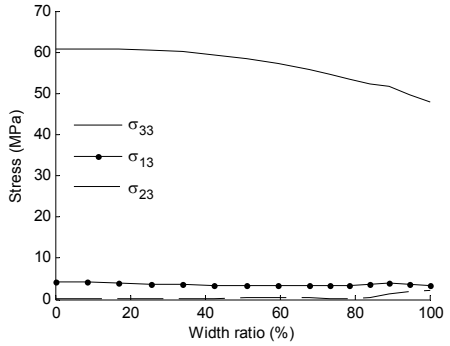

(a) Specimen-1 (r = 6.13 mm, θ = 29°)

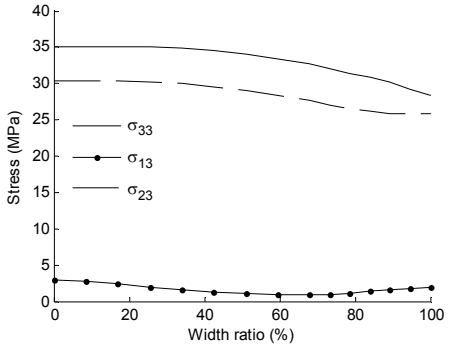

(b) Specimen-2 (r = 5.94 mm, θ = 28°)

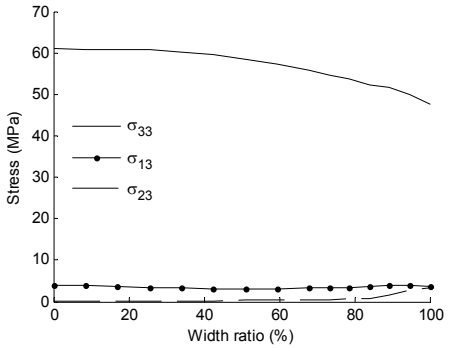

(c) Specimen-3 (r = 5.94 mm, θ = 28°)

Fig. 9 The out-of-plane stresses along the width direction

plane and the free surface of the three curved laminates along the radial direction R, shown in Fig. 8.

Fig. 10(a) shows the stress distributions around the curved region of the specimen-1 along the radial direction. From the figure, it can be seen that the σ_{33} on the symmetric plane and the free surface are high, while the σ_{13} and σ_{23} on the symmetric plane and the free surface are low. The σ_{33} on the symmetric plane is higher than that on the free surface. From the inner surface to the outer surface of the curved laminate, the values of σ_{33} increase firstly and reach a maximum value of about 60 MPa at the sixth ply, then decrease to about 5 MPa on the free surface. This hints that the

delamination should be initiated at the sixth ply for the undamaged curved laminate, which matches with the failure mode of the specimen, shown in Fig. 4(a).

Fig. 10(b) exhibits the stress distributions around the curved region of the specimen-2 along the radial direction. From the figure, it can be seen that the σ_{13} is low, and the σ_{33} and σ_{23} are quite high, with the highest stress about 35 MPa. Here, the σ_{33} is higher than the σ_{23}, whilst the values of σ_{33} and σ_{23} follow the similar trend as those of σ_{33} of specimen-1, which is to say that the values of σ_{33} and σ_{23} increase firstly to their maximum at the sixth ply of the laminate and then decrease to about 5 MPa on the free surface. Therefore, the delamination should be initiated at the sixth ply of the

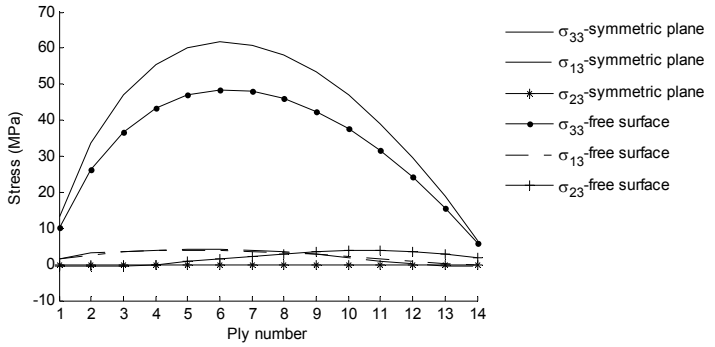

(a) Specimen-1 ($\theta = 29°$)

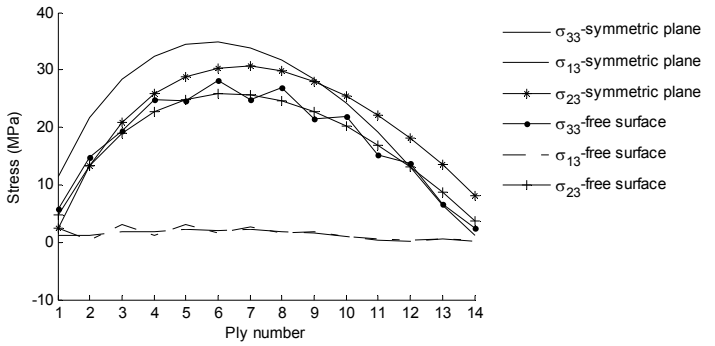

(b) Specimen-2 ($\theta = 28°$)

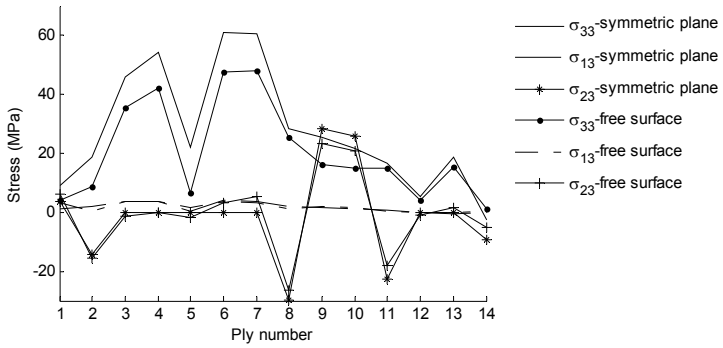

(c) Specimen-3 ($\theta = 28°$)

Fig. 10 The stress distributions along the radial direction

laminate, which also matches with the failure mode of the specimen, shown in Fig. 4(b).

Fig. 10(c) displays the stress distributions around the curved region of the specimen-3 along the radial direction. From the figure, it is clear that the stress distribution curves are not as smooth as those of the specimen-1 and specimen-2, i.e., there are some fluctuations The stress values of σ_{33} on the symmetric plane and free surface increase with the ply number, but decrease greatly at the fifth ply (the ply angle of which is 90°); further reach to the maximum at the sixth ply. The σ_{23} also changes significantly with the ply number; the σ_{23} decreases greatly to about -30 MPa at the eighth ply (the ply angle of which is -45°), and increases greatly to about 30 MPa at the ninth ply, and

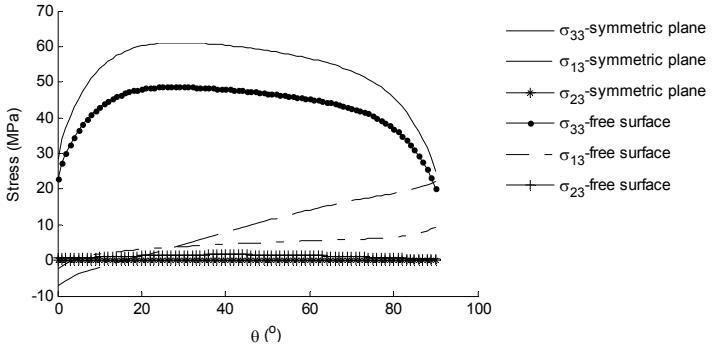

(a) Specimen-1 (r = 6.13 mm)

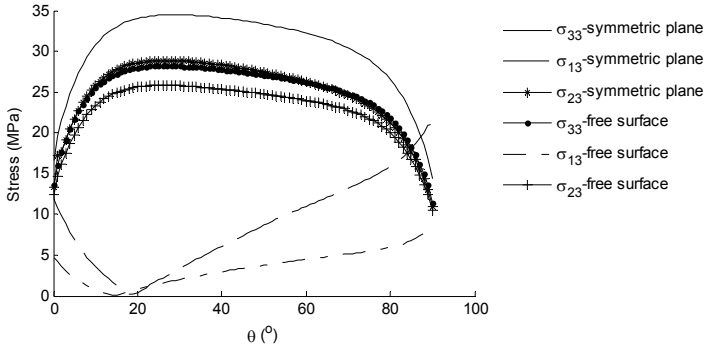

(b) Specimen-2 (r = 5.94 mm)

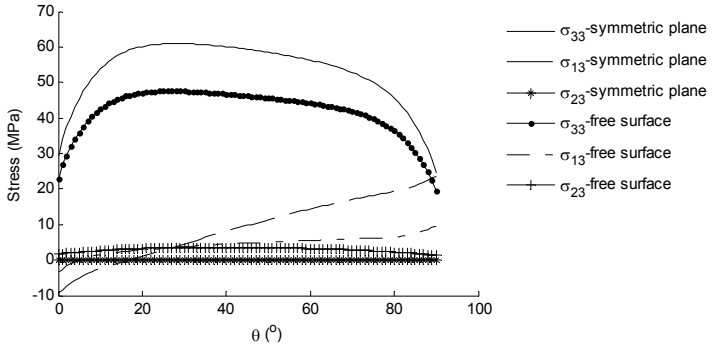

(c) Specimen-3 (r = 5.94 mm)

Fig. 11 The stress distributions along the circumferential direction

then decreases a lot at the eleventh ply. This explains the reason that there are multi-location delaminations on the specimen-3, which is shown in Fig. 4(c).

The onset of the delamination is at the $(R\text{-}r_i)/t$ = 0.42 for the unidirectional right-angled composite laminate according to Wan *et al*. (2013). In other words, the delamination initiates at R = 6.105 mm for the specified unidirectional composite laminate, i.e., specimen-1 in this study. The adjacent ply related to the 6.105 mm radius is the sixth one. Therefore, the location of the onset delamination in the thickness direction obtained from the 3D FEM model in this study is the same with that obtained by using the close form solution and the 2D FEM model (Wan *et al*. 2013). As for the cross-plied curved composite laminates, since the stress, σ_{23}, cannot be obtained by using the closed form solution and the 2D FEM, a 3D FEM is necessary to predict the failure and the stress distribution around the curve region of the laminates.

3) The stress distributions along the circumferential direction

Fig. 11 shows the stress distributions along the circumferential direction in the curved region of the three specimens. From the figure, it can be seen that the stress values of σ_{33} are higher than the stress values of σ_{13} and σ_{23} in most of the curved region. Here, the values of σ_{33} of the three specimens increase firstly with the increase of the θ and reach the maximum at about 29°, and then decrease with the increase of θ. Thus, the delamination is likely initiated at about 29° for the undamaged curved laminates in this application.

The distributions of σ_{13} of specimen-1 and specimen-3 follow the similar pattern. The value of σ_{13} at 0° is about -8 MPa, then increases with the increase of θ, and finally reaches about 20 MPa at 90°. The distribution of σ_{13} of specimen-2 follows different manner. The value of σ_{13} at 0° is about 10 MPa, then decreases with the increase of θ, and reaches about 0 MPa at 19°. Subsequently, the σ_{13} increases with the increase of θ, and gets to 20 MPa at 90°. The stress values of σ_{23} of specimen-1 and specimen-3 are very small, close to zero. Nevertheless, the stress values of σ_{23} of specimen-2, which has $[+/-45]_7$ stacking sequence, are quite high and will play a large role on the failure of the curved laminate.

The onset of the delamination is at θ = 25° according to the FEM provided by Lin (2010). However, considering the nonlinear loading in practical applications, the onset of the delamination should be at θ = 29° according to the FE simulation results of this study for the undamaged curved unidirectional curved laminates.

Through analyzing both the FE simulations and test results on the load-displacement curves, load-strain curves, stress distributions and failure modes, it is found that the simulation results agree with the test results very well. This indicates the validity of the 3D FE models developed on predicting the mechanical behavior of the curved laminates.

4. Discussions

Both the stacking sequences and the ply numbers of the curved laminates can influence their mechanical behavior under tensile loading, which is discussed below.

4.1 Effects of the stacking sequence

The load carrying capacities and the stiffness of the three curved laminates with the same number of plies but different stacking sequences (Table 1) are shown in Table 3. From the table, it can be seen that, among these three specimens, the curved laminate with the stacking sequence of

Table 3 The load capacities and the stiffness of cured laminate with different lay-ups

Laminates	Specimen-1	Specimen-2	Specimen-3
Load capacity (N)	1800	1901	1739
Stiffness (N/mm)	683	713	710

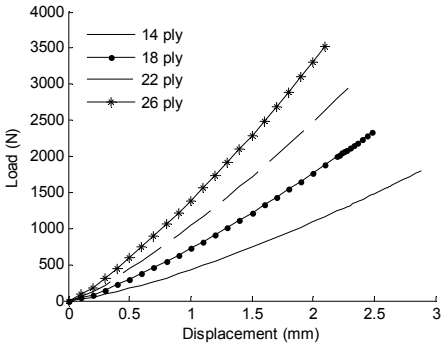

Fig. 12 Load-displacement curves of the specimens with different thickness

Table 4 The load carrying capacities and the stiffness of the curved laminates with different number of plies

Laminates	$[0]_{14}$	$[0]_{18}$	$[0]_{22}$	$[0]_{26}$
Load capacity (N)	1800	2335	2965	3530
Stiffness (N/mm)	683	1026	1405	1837

$[+/45]_7$ (Specimen-2) has higher load carrying capacity and stiffness than other two specimens. The curved laminate with the stacking sequence of $[0]_{14}$ (Specimen-1) has the lowest stiffness, and the curved laminate with the stacking sequence of [+/-45, 0_2, 90, 0_2, -/+45, +/-45, 90, 0, -45] (Specimen-3) has the lowest load carrying capacity. The differences between the maximum and the minimum load carrying capacities and stiffnesses are 9.3 % and 4.4 %, respectively.

Though the interlaminar shear stress (produced by the material property mismatch between the adjacent plies of the cross plied composite laminates) makes a significant contribution to the delamination failure of the curved laminates, the use of multidirectional composites does not decrease the load carrying capacity of the laminates compared with the unidirectional ones.

4.2 Effects of the thickness of the laminates

The unidirectional curved laminates with different ply numbers subjected to the same load condition (Fig. 2) are simulated by using the FEM described in Section 3. Fig. 12 shows the comparison of the load-displacement curves of the $[0]_{14}$, $[0]_{18}$, $[0]_{22}$, and $[0]_{26}$ laminates. The load carrying capacities and the stiffnesses of the four different curved laminates are shown in Table 4.

From Fig. 12 and Table 4, it can be seen that both the load carrying capacity and the stiffness of the curved laminates increase with the increase of the number of ply, as expected.

Nevertheless, the load carrying capacities per ply for the four different curved laminates are 129, 130, 135 and 136 N, and the stiffness per ply re 48.8, 57.0, 63.9 and 70.6 N/mm. Therefore, the load carrying capacities of the curved laminates are almost proportional to the thickness. Here,

the increase of the load carrying capacity is mild with the ply number. However, the increase on the stiffness is much more significant with the number of plies.

4.3 Comparison with the aluminum curved structures

The mechanical behavior of the 2.632 mm thick and 4.888 mm thick right-angled brackets made of 2024-T3 aluminum alloy, which have the same thickness with the $[0]_{14}$ and $[0]_{26}$ composite laminates, are also simulated by using the FEM proposed in this paper. The mechanical properties of the aluminum alloy can be referred to Mil-handbook (2003). The maximum distortion energy theory (von Mises) is used to predict the failure of aluminum material and the aluminum brackets are judged as failure when the von Mises stress reaches 324 MPa.

The load versus displacement curves of the two aluminum curved structures are shown in Fig. 13. The strengths of the two aluminum curved structures are 979 N and 2542 N, respectively, and the stiffnesses are 456 N/mm and 1511 N/mm, respectively. Both the strength and stiffness of the aluminum curved brackets are lower than those of the composite curved brackets with the same thickness. Moreover, the density of the composite material, 1.8 g/mm^3, is lower than that of the aluminum alloy, 2.7 g/mm^3. Therefore, the composite curved brackets have higher weight saving potential than the aluminum brackets, though the composite curved brackets do not take full advantages of their performance because of the delamination failure.

The strength per unit thickness of the aluminum curved structures increase with the increase of the total thickness and the increasing rate on the curved aluminum structure is larger than that on

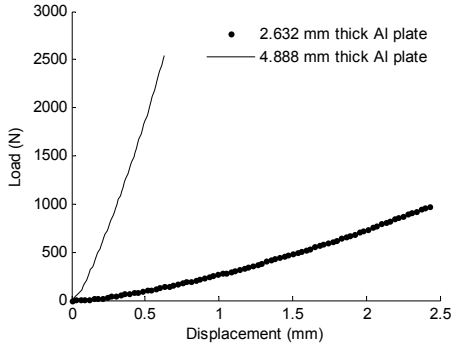

Fig. 13 Load-displacement curves of the Aluminum curved structure

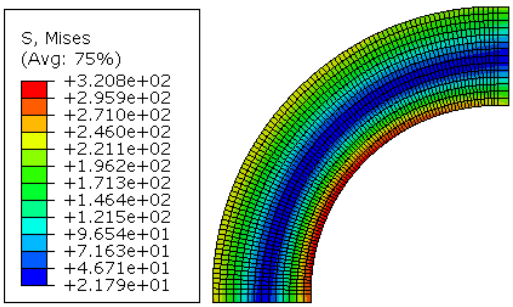

Fig. 14 Stress (MPa) state around the curved region of the 2.632 mm thick aluminum bracket

the curved composite structure. Therefore, the increase on both the strength and the stiffness of the composite curved structures is not as large as those of the aluminum curved structures if only the same thickness is increased. The load carrying efficiency of the curved metallic shear tie will exceed the composite ones if the bracket is thick enough. The reason is due to the difference on the failure criteria and stress distribution along the thickness direction between the composite and aluminum curved brackets. Before it fails, the von Mises stress state around the curved region of the 2.632 mm thick aluminum curved bracket is shown in Fig. 14, as an example. From the figure, it can be drawn that under shear loading the curved aluminum beam deforms non-linearly or even fractures due to the von Mises stress at the inner radius around the curved region exceeding the limit. However, the aluminum beam delaminates at a certain depth along the thickness direction, because of out-of-plane stress.

5. Conclusions

The mechanical behavior of right-angled laminates with different lay-ups and thicknesses are studied in this paper. Through the analyses, it can be concluded that:

- Delamination introduced by the out-of-plane normal tensile stress around the curved region is the primary failure mode of the curved laminates in practical applications, where the delamination initiates abruptly and develops quickly.
- The onset of the delamination of the three curved laminates with the same ply number is all initiated on the middle plane of the bracket along width direction, about 29^{o} along the circumferential direction and close to the inner surface.
- The stacking sequence has little effect on the load carrying capacity, but will have more effect on the stiffness of the curved composite laminates.
- The curved composite brackets investigated have the higher weight saving potential than the aluminum ones. However, with the increase of thickness, the advantages of the composite material decrease in the form of curved structure.

Acknowledgments

The research described in this paper was financially supported by the CAST Innovation Foundation (14GFZ-JJ04-069) and the HT Support Foundation (14GFZ-JJ02-043).

References

ASTM Committee (2007), ASTM D 6415/D 6415M-06: Standard test method for measuring the curved beam strength of a fiber-reinforced polymer-matrix composite.

Chang, F. and Springer, G.S. (1986), "The strength of fiber reinforced composite bends", *J. Compos. Mater.*, **20**(1), 30-45.

Cui, W.C., Liu, T., Len, J.X. and Ruo, R. (1996), "Interlaminar Tensile Strength (ILTS) measurement of woven glass/polyester laminates using four-point curved beam specimen", *Compos. Part A*, **27**(11), 1097-1105.

Herrington, P.D. and Sabbaghian, M. (1991), "Factors affecting the friction coefficients between metallic washers and composite surfaces", *Compos.*, **22**(6), 418-424.

Hibbitt, D., Karlsson, B. and Sorensen, P. (2011), ABAQUS documents (version 6.10), Dassault Systemes

Simulia Corporation, Providence, RI, USA.
Joh, D. (1990), "A semi-micromechanic interlaminar strain analysis on curved-beam specimens", NASA Contactor report-NASA CR; 189512.
Lekhnitskii, S.G. (1987), *Anisotropic Plates*, (3rd Edition), Gordon and Breach Science Publishers, New York, NY, USA.
Lin, C.W. (2010), "Finite deformation of 2-D thin circular curved laminated beams", *Hsiuping J*., **22**, 19-34.
Lin, K.C and Hsieh, C.M. (2007), "The closed form general solutions of 2-D curved laminated beams of variable curvatures", *Compos*. *Struct*., **79**(4), 606-618.
Lin, K.C. and Hsieh, C.M. (2011), "Finite deformation of 2-D laminated curved beams with variable curvatures", *Int*. *J*. *Non-Linear Mech*., **46**(10), 1293-1304.
Mechanical Properties of CYCOM® 977-2-35%-24KIMS-198-600, Technical Service Cytec Engineered Materials.
Miao, Y., Li, J., Gong, Z., Xu, J., He, K., Peng, J. and Cui, Y. (2013), "Study on the effect of cure cycle on the process induced deformation of cap shaped stiffened composite panels", *Appl*. *Compos*. *Mater*., **20**(4), 709-718.
Military Handbook--MIL-HDBK-5F (2003), *Metallic Materials and Elements for Aerospace Vehicle Structures*, Department of Defense, USA.
Mukundan, S. (2003), "Structural design and analysis of a lightweight composite sandwich space radiator panel", Master Thesis; Mechanical Engineering, Texas A&M University, TX, USA.
Ng, S.P., Tse, P.C. and Lau, K.J. (2001), "Progressive failure analysis of 2/2 twill weave fabric composites with moulded-in circular hole", *Compos*. *Part B-Eng*., **32**(2), 139-152.
Nguyen, T. (2010), "Effects of curvature on the stresses of a curved laminated beams subjected to bending", Master thesis, The University of Texas at Arlington, Arlington, TX, USA.
Padhi, G.S., McCarthy, M.A. and McCarthy, C.T. (2002), "BOLJAT: a tool for designing composite bolted joints using three-dimensional finite element analysis", *Compos*. *Part A*, **33**, 1573-1584.
Roos, R. (2008), "Model for interlaminar normal stress in doubly curved laminates", Ph.D. Dissertation; Swiss Federal Institute of Technology, Zurich, Swiss.
Rosales-Iriarte, F., Fellows, N.A. and Durodola, J.F. (2012), "Failure prediction in carbon compression subjected to bearing versus bypass loading", *J*. *Compos*. *Mater*., **46**(15), 1859-1878.
Shimizu, T. and Abe, T. (2013), "Tool material effects on process induced deformation of composite spar structures", *Proceedings of the 19th International Conference on Composite Materials*, Montreal, Canada, August, pp. 1003-1010.
Sorrentino, L. and Bellini, C. (2013), "Numerical study of compaction influence on spring-in of thin composite components manufactured by vacuum bag process", *Proceedings of the 19th International Conference on Composite Materials*, Montreal, Canada, August, pp. 9095-9103.
Sun, J., Gu, Y.Z., Li, M., Li, Y.X. and Zhang, Z.G. (2013), "Relationship between slipping friction prepreg stacks and forming quality of hot diaphragm formed c-shaped thermosetting composite laminates", *Proceedings of the 19th International Conference on Composite Materials*, Montreal, Canada, August, pp. 3066-3075.
Wan, Y., Goto, T., Matsuo, T., Takahashi, J. and Ohsawa, I. (2013), "Investigation about fracture mode and strength in curved section of carbon fiber reinforced polypropylene", *Proceedings of the 19th International Conference on Composite Materials*, Montreal, Canada, August, pp. 6695-6702.
Wimmer, G., Kitzmuller, W., Pinter, G., Wettermann, T. and Pettermann, H.E. (2009), "Computational and experimental investigation ofdelamination in L-shaped laminated composite components", *Eng*. *Fract*. *Mech*., **76**(18), 2810-2820.
Wisnow, M.R., Petrossian, Z.J. and Jones, M.I. (1996), "Interlaminar failure of unidirectional glass/epoxy due to combined through thickness shear and tension", *Compos*. *Part A*, **27**(10), 921-929.
Ye, L. (1988), "Role of matrix resin in delamination onset and growth in composite laminates", *Compos*. *Sci*. *Technol*., **33**(4), 257-277.

CC